ISBN: 978-3-95450-247-9 ISSN: 2673-5490 doi: 10.18429/JACoW-IPAC2024-MOPR72

TRANSPORT AND DOSIMETRY OF LASER-DRIVEN PROTON BEAMS FOR RADIOBIOLOGY AT THE BELLA CENTER *

J.T. De Chant[1†], L. Obst-Huebl, K. Nakamura, S. Hakimi, A. McIlvenny, S. Barber, J. Inman, A. M. Snijders, A. J. Gonsalves, J. van Tilborg, C. G. R. Geddes, C. B. Schroeder, E. Esarey,
Lawrence Berkeley National Laboratory, Berkeley, CA, USA
B. Stassel, University of Michigan, Ann Arbor, MI, USA
C. Palmer, Queen's University Belfast, Belfast, UK
[1]also at Michigan State University, East Lansing, MI, USA

Abstract

Laser-driven ion accelerators (LDIAs) are well-suited for radiobiological research on ultra-high dose rate effects due to their high intensity. For this application, a transport system is required to deliver the desired beam intensity and dose distribution to a sample site while online dosimetry is required due to the inherent shot-to-shot variability of LDIAs. At the BELLA Center's iP2 beamline, we implemented two compact, permanent magnet-based beam transport configurations for delivering 10 or 30 MeV protons to a biological sample, along with a suite of diagnostics used for dosimetry. These diagnostics include multiple integrating current transformers (ICTs) for indirect online dose measurements and calibrated radiochromic films (RCFs) to measure the dose profile and calibrate the ICT dosimetry. Monte-Carlo (MC) simulations of the beamline allow us to predict the dose received by the sample and correct the linear energy transfer (LET)-dependent response of the RCFs. This work not only further establishes the practicality of utilizing LDIAs for radiobiological research but also highlights the BELLA Center's capability to accommodate further experiments in this domain.

INTRODUCTION

Laser-driven ion accelerators (LDIAs) have garnered attention across various disciplines due to their unique beam properties, which hold potential for a wide range of applications. In laser–driven (LD) ion acceleration, a high intensity laser pulse ($> 10^{19}$ W/cm^2) interacts with a thin solid target and generates a plasma that can sustain high accelerating gradients (10s-1000s GeV/cm) [1]. A large number of ions can be accelerated in these fields to very high energies over short distances (sub mm) through various different mechanisms. This acceleration technique stands out from conventional RF-driven ion acceleration due to its high ion production ($\sim 10^{13}$ ions per shot) and ultra short bunch length (~ps at the source) [2].

Recently, LDIAs have been utlized to explore the benefits of ultra-high dose rates in radiotherapy [3, 4]. Irradiations with high dose rates $\geq$ 40 Gy/s have been shown to induce sparing of healthy tissues while maintaining equal tumor killing compared to conventional dose rate irradiations [5]. This so-called "FLASH effect" is currently not well understood and its underlying mechanisms have not been fully explored due to limited access to conventional radiation sources that can achieve the necessary dose rates [6]. Due to the high intensity beams they create, LDIAs are well-suited to explore this effect. They also offer other potential benefits for use in radiotherapy. Their broadband energy spectra can be shaped to spread out the Bragg peak of the energy deposition, allowing for irradiation over a larger depth than with a conventional pencil beam scanning [7]. Additionally, LD ion beams consist of multiple species, enabling access to different regimes of biological effectiveness.

To utilize LDIAs for radiotherapy, the beams must be efficiently collected and transported to the sample location while maintaining their high intensity to achieve a high dose rate and uniform beam profile. The dose delivered to the sample also needs to be precisely monitored due to the inherent shot-to-shot variability of LDIAs [8].

Presented here is the implementation and simulation of two compact, permanent magnet-based beam transport configurations for delivering 10 or 30 MeV protons to *in vivo* biological samples that were used at the BELLA Center's iP2 beamline [9] in a recent experimental campaign to explore ultra-high dose rate effects. Also presented are the multiple ways we performed and verified the doses delivered to the samples.

PROTON BEAMLINE SIMULATIONS

The design of the proton transport system was performed with a homemade MATLAB simulation code that combines the features of a traditional map code, through the integration of COSY INFINITY [10], with a Monte Carlo (MC) based radiation transport code. This code calculates the trajectories of a large number of particles and models the energy deposition into matter along the beam path and allows for the optimization of the dose delivered to the biological sample to ensure a high dose per shot and a uniform dose profile.

The code works by first generating a large number of macroparticles ($> 10^6$) with initial parameters to match the

* Work was supported by U.S. DOE-OS, FES, and HEP under DE-AC02-05CH11231, and by LaserNetUS. J. D. was supported by DOE-OS, HEP under DE-SC0018362 and MSU. S. H. was supported by the DOE-FES Postdoctoral Research Program, administered by ORISE DE-SC0014664.B. Stassel was supported by the U.S. DOE-OS, WDTS, SCGSR program, also administered by ORISE.
† jtdechant@lbl.gov

ISBN: 978-3-95450-247-9 ISSN: 2673-5490 doi: 10.18429/JACoW-IPAC2024-MOPR72

beam emerging from the laser-plasma interaction, based on previous experiments and other LDIAs [3, 9, 11]. These particles are then propagated through a high order transfer map, generated using COSY, that describes their propagation through the various beam optics and drift spaces. We found that a 4th order mapping or above is necessary to fully capture the dynamics of the LD beam, given its large energy spread and initial divergence.

The code then models the propagation of the particles through the various materials along the beam path on their way to the biological sample, as well as the energy deposition inside the sample. This modeling accounts for effects of energy degradation and scattering on the beam spectrum and profile, while describing the dose deposition on the sample and a number of radiochromic films (RCF) placed in the beam for dosimetry, based on data from the Particle Data Group [12]. The beamline setup and and all relevant absorbers are described in the next section. A comparison of the simulated dose profile at the sample location and the dose profile measured with RCF is shown in Fig. 1 and shows good agreement of the overall shape.

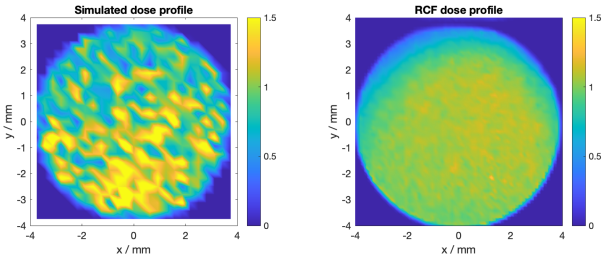

Figure 1: Comparison of simulated dose profile (left) and measured dose profile (right) at the sample location. The simulated profile reproduces the slight gradient at the top edge of the irradiation area. The speckled pattern is due to the low number of macroparticles simulated that make it to the sample location, but the dose uniformity and magnitude does converge with higher resolution simulations. Both profiles are normalized to their mean dose value.

These simulations also proved necessary for the dosimetry due to the linear energy transfer (LET) dependent response of the RCFs. Schollmeier et al [13] has shown that, like other charged particle detectors, the RCF response is affected by LET, causing films to under-respond near the Bragg peak where the LET is highest. Schollmeier et al. found that the film detection efficiency η, the ratio of the measured dose to the expected dose, falls with increasing stopping power $\mathrm{d}E/\mathrm{d}x$ as

$$\eta = 1 - 0.4e^{-4\exp -0.2\mathrm{d}E/\mathrm{d}x}. \quad (1)$$

The stopping power for a given material is a function of the incident particle energy and the material properties. Lookup tables for many common materials are available through the NIST database [14].

Using Eq. 1 and the beam spectrum modeled with the MC code, the dose values measured by the RCFs were scaled to account for this LET effect.

EXPERIMENTAL SETUP AND BEAM TRANSPORT

An illustration of the proton beamline and experimental setup is shown in Fig. 2. The BELLA PW laser was used to deliver pulses with 22 J pulse energy and 37 fs pulse length to a custom-designed tape drive target system at high rep rate (0.2 Hz). The protons were accelerated in the laser-plasma interaction via Target Normal Sheath Acceleration (TNSA).

A set of compact, permanent magnet quadrupoles (PMQs) were used for beam transport that had two configurations designed to collimate 10 MeV and 29 MeV proton beams, respectively. The PMQs achieve a high field strength (hundreds T/m) with a relatively large bore (20-50 mm), enabling efficient capture and collimation of the ion beam [15]. The first two PMQs were designed to collimate 10 MeV protons. A second set of PMQs could be moved into the beam path using linear stages to increase the overall focusing strength of the transport and for collimation of 29 MeV protons. The 29 MeV configuration allows the iP2 beamline to irradiate samples at larger penetration depths. After collimation, the beam is deflected downward by a permanent magnet dipole (0.5 T) for energy selection and spatial separation from the co-propagating neutrals and electrons.

The beam transport was designed to deliver as much dose to the sample (mouse ear) as possible with a compact permanent magnet system while maintaining a homogeneous dose distribution, both transversely and longitudinally at the sample site. To ensure longitudinal dose uniformity in penetrating the sample, there is a need to balance the energy spectrum so as to maximize the total charge delivered while applying an energy spectrum well away from the Bragg peak. The energy spectrum of the beam at the source is Maxwellian so the vast majority of the beam is of low energy (< 10 MeV) and collecting only a small fraction (<1%) of this part of the spectrum is enough to outweigh the energy deposited on the sample by the higher energy particles.

The energy spectrum of the beam delivered to the sample was measured using a stack of calibrated RCF (Gafchromic, EBT3) and is shown in Fig. 3. The process of unfolding the beam spectrum from the stacks is outlined in [13, 16], and the correction factor η for the LET related sensitivity reduction was applied. There is an unexpected peak in the spectrum at $\sim$ 7 MeV that was not present in the simulations of the beamline at that point. This is likely due to the transfer map representation of the beam dynamics being centered around a reference particle energy, E_0 = 28.5 MeV, far away from this portion of the spectrum. Protons with energies near this peak would be close to their Bragg peak at the sample location and would thus dominate the dose deposited. While this complicated the dosimetry, the RCFs placed before and after the sample during irradiation allowed for us to see the impact of the spectrum on the dose profile. Future work on the beamline design and the simulations will address this difference between measured and simulated spectrum at the sample.

ISBN: 978-3-95450-247-9 ISSN: 2673-5490 doi: 10.18429/JACoW-IPAC2024-MOPR72

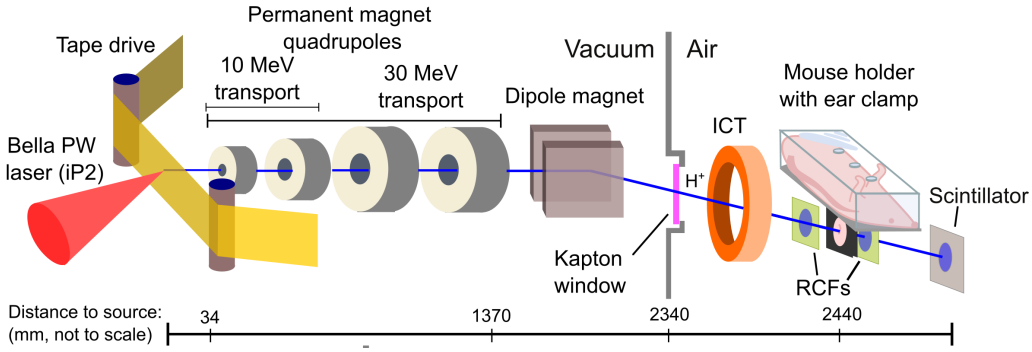

Figure 2: Illustration of experimental setup for mouse ear irradiations. Components and distances are not to scale. The beam transport has two configurations designed to collimate 10 MeV and 28.5 MeV proton beams, respectively. The quadrupole magnets are mounted to motorized stages to easily switch from the 10 MeV transport to the 30 MeV transport by moving the additional quads into the beam path. The ICT is used to perform online dosimetry and is calibrated against RCFs placed at the sample location. RCFs are placed in front and behind each individual mouse ear sample during irradiation to verify the delivered dose.

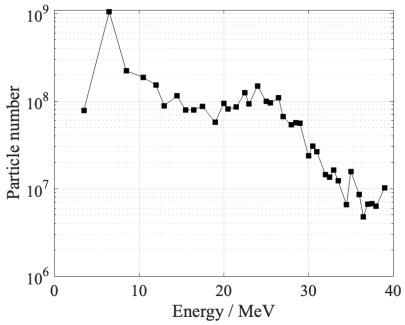

Figure 3: Beam spectrum measured upstream of the sample location using a stack of EBT3 RCF.

DIAGNOSTICS FOR DOSIMETRY

Dosimetry was performed during irradiation and verified after through a combination of on-shot charge measurements with an Integrating Current Transformer (ICT) and accumulated dose measurements with RCFs as shown in 2. Before irradiations of biological samples began, and at least once per day over the course of the campaign, the dose measured by an *in situ* RCF placed into the sample holder was correlated to the summed charge measured by the ICT over multiple shots to establish a charge-to-dose conversion, similar to the process outlined in [8]. This allowed us to monitor the dose we delivered to the sample on each shot and determine the number of shots needed to reach the prescribed dose for each sample.

Concurrently, a set of RCFs were placed directly in front (RCF-A) and behind (RCF-C) the *in situ* RCF (RCF-B) at the sample location during the ICT calibration shots to obtain conversion factors between the doses measured by RCFs A and C to the sample dose. Subsequently, RCFs A and C were also placed in front and behind each of the samples during irradiation to verify the dose applied to each sample.

In order to obtain the actual dose measured by each RCF, the raw dose values were scaled according to the film detection efficiency η. The average stopping power of the beam at each of the RCFs was estimated by inputting the energy spectrum shown in Fig. 3 into the in-air portion of MC code. The film detection efficiency for each RCF was estimated to be $\eta = 0.767, 0.754, 0.804$ for RCFs A, B, and C respectively. To obtain the actual dose delivered to the sample, D_S, the doses measured by RCFs A and C for each sample, D_A and D_C, were scaled by the ratio of the doses measured by RCFs A and C, D_A* and D_C*, to the dose measured by the *in situ* RCF-B, D_B* for each day:

$$D_S = \frac{1}{2}\left(D_A\frac{D_B*}{D_A*} + D_C\frac{D_B*}{D_C*}\right). \quad (2)$$

After the initial guidance provided by online charge measurements, this RCF analysis routine allowed us to determine the absolute dose delivered to each sample. The applied doses ranged from approximately 30-70 Gy, with a sample-to-sample dose variation of ~ 10 % (standard deviation) within each day of the campaign. This variation partly results from changes in the proton spectrum over the course of a day, affecting the charge-to-dose calibration of the online dosimetry. Improving the stability of the proton spectrum is the subject of ongoing work and the details will be discussed in a future publication.

CONCLUSION

The implementation of beam transport configurations and dosimetry tools at the BELLA Center's iP2 beamline represents a significant advancement in utilizing LDIAs for radiobiological research. Compact, permanent magnet-based configurations allowed precise and high-intensity proton delivery. The BELLA Center has demonstrated its capacity for further experiments in radiobiological research, exploring ultra-high dose rate effects like the FLASH effect. Future research will focus on refining beam transport and dosimetry systems and advancing LDIA technology for more comprehensive radiobiological studies.

ISBN: 978-3-95450-247-9 ISSN: 2673-5490 doi: 10.18429/JACoW-IPAC2024-MOPR72

REFERENCES

[1] J. Badziak, "Laser-driven ion acceleration: Methods, challenges and prospects," *Journal of Physics: Conference Series*, vol. 959, no. 1, p. 012 001, 2018. doi:10.1088/1742-6596/959/1/012001

[2] A. Macchi, M. Borghesi, and M. Passoni, "Ion acceleration by superintense laser-plasma interaction," *Rev. Mod. Phys.*, vol. 85, pp. 751–793, 2 2013. doi:10.1103/RevModPhys.85.751

[3] J. Bin *et al.*, "A new platform for ultra-high dose rate radiobiological research using the bella pw laser proton beamline," *Scientific Reports*, vol. 12, no. 1, 2022. doi:10.1038/s41598-022-05181-3

[4] J. Metzkes-Ng *et al.*, "The dresden platform is a research hub for ultra-high dose rate radiobiology," *Scientific Reports*, vol. 13, no. 1, p. 20 611, 2023.

[5] V. Favaudon *et al.*, "Ultrahigh dose-rate flash irradiation increases the differential response between normal and tumor tissue in mice," *Science Translational Medicine*, vol. 6, no. 245, 245ra93–245ra93, 2014. doi:10.1126/scitranslmed.3008973

[6] R. Schulte *et al.*, "Transformative technology for flash radiation therapy," *Applied Sciences*, vol. 13, no. 8, 2023. doi:10.3390/app13085021

[7] E. Pedroni, "Pencil beam scanning," *Proton and Charged Particle Radiotherapy*, vol. 42, p. 40, 2008.

[8] L. D. Geulig *et al.*, "Online charge measurement for petawatt laser-driven ion acceleration," *Review of Scientific Instruments*, vol. 93, no. 10, p. 103 301, 2022. doi:10.1063/5.0096423

[9] L. Obst-Huebl *et al.*, "High power commissioning of BELLA iP2 up to 17 J," in *Applying Laser-driven Particle Acceleration III: Using Distinctive Energetic Particle and Photon Sources*, International Society for Optics and Photonics, vol. 12583, 2023, p. 1 258 305. doi:10.1117/12.2669162

[10] M. B. Kyoko Makino, "Cosy infinity version 9," *Nuclear Instruments and Methods*, vol. A558, pp. 346–350, 2005.

[11] A. Macchi, M. Borghesi, and M. Passoni, "Ion acceleration by superintense laser-plasma interaction," *Rev. Mod. Phys.*, vol. 85, pp. 751–793, 2 2013. doi:10.1103/RevModPhys.85.751

[12] R. L. Workman *et al.*, "Review of Particle Physics," *PTEP*, vol. 2022, p. 083C01, 2022. doi:10.1093/ptep/ptac097

[13] M. Schollmeier, M. Geissel, A. B. Sefkow, and K. A. Flippo, "Improved spectral data unfolding for radiochromic film imaging spectroscopy of laser-accelerated proton beams," *Review of Scientific Instruments*, vol. 85, no. 4, p. 043 305, 2014. doi:10.1063/1.4870895

[14] M. J. Berger, J. S. Coursey, M. A. Zucker, and J. Chang, "Stopping-power and range tables for electrons, protons, and helium ions," National Institute of Standards and Technology, Tech. Rep. NIST Standard Reference Database 124, 2017. doi:10.18434/T4NC7P

[15] K. Halbach, "Design of permanent multipole magnets with oriented rare earth cobalt material," *Nuclear Instruments and Methods*, vol. 169, no. 1, pp. 1–10, 1980. doi:10.1016/0029-554X(80)90094-4

[16] J. H. Bin *et al.*, "Absolute calibration of GafChromic film for very high flux laser driven ion beams," *Review of Scientific Instruments*, vol. 90, no. 5, p. 053 301, 2019. doi:10.1063/1.5086822